Turbulent open-channel flow with upward seepage

Écoulement turbulent en canal découvert avec un fond poreux

NIAN-SHENG CHENG, *Department of Hydrodynamics and Water Resources, Technical University of Denmark, Lyngby 2800, Denmark*

YEE-MENG CHIEW, *School of Civil and Structural Engineering, Nanyang Technological University, Nanyang Avenue, Singapore 639798*

ABSTRACT

Measurements of turbulent open-channel flow subjected to an upward bed seepage were performed in a laboratory flume using a two-dimensional Acoustic Doppler Velocimeter and a minipropeller. The experimental results show that the boundary seepage affects the time-mean streamwise velocity, the rms values of the velocity fluctuations, the Reynolds shear stress and the bed shear stress in open-channel flow. Along the seepage zone, the mean streamwise velocity increases much more in the surface layer than that in the near-bed region, whereas the turbulent intensities and Reynolds shear stress increase significantly in the near-bed region. The bed shear stress that was computed using the momentum integral equation shows a steady reduction with increasing upward seepage velocity.

RÉSUMÉ

Des mesures d'écoulement turbulent en canal découvert avec un lit permettant des écoulements de filtration sur la verticale ont été réalisées dans un canal de laboratoire avec un vélocimètre laser à deux dimensions ainsi qu'avec un micromoulinet. Les résultats expérimentaux montrent que les infiltrations au fond affectent la vitesse moyenne d'écoulement, les moyennes quadratiques des fluctuations de vitesse, les contraintes de Reynolds et la contrainte ce cisaillement. Au long de la zone d'échange par infiltration, la vitesse moyenne débitante croît plus dans la couche de surface qu'au voisinage du fond, tandis que l'intensité de turbulence et les contraintes de Reynolds croissent de façon significative au voisinage du fond. La contrainte de cisaillement à la paroi, calculée à partir de l'équation intégrale de quantité de mouvement, montre une diminution constante au fur et à mesure que la vitesse verticale de filtration croît.

1 Introduction

Permeable boundaries are often encountered in nature. Typical example are porous boundaries consisting of sediment particles in many natural rivers and densely vegetated boundaries in irrigation canals. The permeable boundary enables mass and momentum transfer across the interface between fluid and porous media. The interaction between turbulent flow and a permeable boundary may result in changes in the structural features of the flow, such as velocity profile, turbulence intensity and boundary shear stress, as compared with those in relation to an impermeable boundary. The information associated with these changes is necessary for the study of the effect of seepage on sediment transport over a permeable bed.

Previous studies on turbulent open-channel flows with a boundary seepage can be found in Oldenziel and Brink (1974), Willetts and Drossos (1975), Maclean (1991a, 1991b) and Prinos (1995). Oldenziel and Brink (1974) measured the velocity profiles at the downstream end of a permeable bed. They found that the horizontal velocity near the bed decreases with an upward seepage or injection and increases with a downward seepage or suction. Willetts and Drossos (1975) conducted an experimental study to examine the effect of downward seepage on the streamwise veloc-

Revision received August 16, 1997. Open for discussion till December 31, 1998.

ity profile and local erosion. They proposed an exponential expression to describe the velocity distribution over the seepage zone. Maclean (1991a, 1991b) conducted a series of studies to investigate the velocity profiles and bed shear stresses in open-channel flows subjected to high-rate suction. Maclean (1991a) performed two sets of velocity measurements over the suction zone with high seepage rates. He reported that the velocity gradient in the logarithmic region far away from the bed decreased as the suction velocity increased. To evaluate the bed shear stress with suction, Maclean (1991b) observed the incipient motion of indicator grains with predetermined critical shear stresses. The magnitude of the increased bed shear stress was found to be approximately twice the shear stress without suction when the suction rate was 10% of the mean channel velocity. Prinos (1995) conducted numerical computations using turbulence models to investigate the effect of bed suction on the structure of turbulent open-channel flows. The result shows that the near-bed velocity and the bed shear stress within the seepage region increased with increasing suction rate. However, the predicted increments associated with the bed shear stress were much higher than those obtained by Maclean (1991b).

The objective of this study is to experimentally explore the seepage effect on the variations of the time-mean velocity, the root-mean-square (rms) value of velocity fluctuations, the Reynolds shear stress and the bed shear stress in open-channel flow. In order to evaluate the bed shear stress, a momentum integral equation is also derived and used in this study for a two-dimensional flow subjected to seepage.

2 Experimental arrangement

2.1 *Open-channel flume*

The open-channel flow experiments were conducted in a glass-sided horizontal flume that was 30 m long, 0.7 m wide and 0.6 m deep. Water was circulated through a submersible pump installed in a laboratory reservoir. The flow rate was controlled by a speed inverter and a valve and monitored using an electromagnetic flow meter. Pipe straighteners were installed at the entrance of the channel to prevent the occurrence of large-scale disturbances and to achieve uniform entrance flow. The water depth in the flume was regulated using a tailgate weir. The depth at the test section was measured using an open channel depth gauge, which had a resolution of 0.2 mm. Located at 16 m from the upstream end of the flume was the test section that included a recess 2 m long, 0.7 m wide and 0.4 m deep (see Fig. 1). The recess served as a seepage zone where an upward seepage was applied from its bottom by a second submersible pump that was installed in the laboratory reservoir. The seepage flow rate was determined using a turbine flow meter. Before water seeped into the sediment bed, it was first delivered through perforated pipes that were installed at the lower portion of the recess. Holes with different sizes were drilled along the pipes to ensure a uniform seepage velocity. Above the perforated pipes was a perforated plate, which supported a layer of sediment particles in the seepage zone. A layer of filter net placed on the perforated plate prevented the sand particles from falling into the lower portion of the recess. The beds of the flume both upstream and downstream of the test section were roughened with the same sediment particles as those in the recess. Two uniform sediments with median gain diameter of 1.95 mm and 5.83 mm were used in the study.

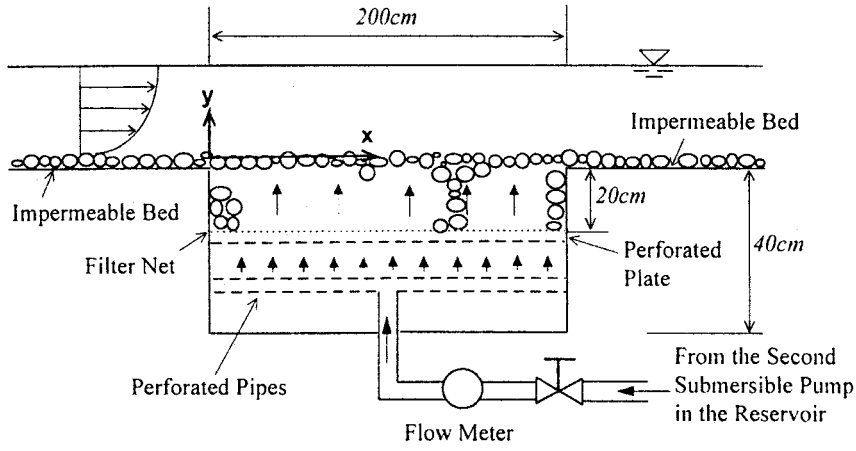

Fig. 1. Schematic diagram of test section.

2.2 *Measurement techniques*

Velocity measurements were performed using a two-dimensional Acoustic Doppler Velocimeter (ADV) and a minipropeller. The ADV system was used to measure two-dimensional instantaneous velocities so that the turbulent properties of flows could be investigated. When only mean velocity was considered, an 8 mm minipropeller current meter was used.

The ADV system applied acoustic sensing techniques to measure flow in a remote sampling volume that was located below the tip of the probe. The instrument comprised three modules: the measuring probe, the conditioning module and the processing module. The acoustic sensor for a two-dimensional probe consisted of one transmitting transducer and two receiving transducers. The transmitting transducer produced periodic short acoustic pulses. As a pulse was sent out into the flow, it intercepted ambient scatter like microbubble and suspended particle as a target. The target scattered the incident pulse in all directions, some being directed towards the receiver. As far as the receiving transducer was concerned, the target had generated (by reflection) an acoustic signal that propagated from the target in a sampling volume. The sampling volume was about 0.9 cm in height and was defined by the intersection of the transmitting and receiving beams. Assuming the target traveled with the velocity of the flow, the Doppler shift corresponding to the relative motion of the target enabled the evaluation of the velocity of the flow. As the ADV measured the flow some distance away from the tip of the probe, different orientations of probes, such as up-looking and down-looking probes, were alternately employed to complete velocity measurements throughout the entire depth of the flow. Because of reflections of the pulses sent by the ADV. it was often necessary to prevent interference from the boundaries around the probe used for measurements. For this purpose, fully rough beds were found to be necessary. After a preliminary test, a coarse sediment of 5.83 mm was used as the bed material. The bed consisting of coarse particles also allowed a high flow velocity while no sand particles were in motion, thus providing another excellent condition for ADV operations.

When only time-mean streamwise velocity was required, the minipropeller with a diameter of 8 mm was used instead. The minipropeller current meter was designed to measure velocity in the range of 4 to 300 cm/s. Measurements of the mean velocity obtained from both the ADV and the minipropeller, respectively, were found to agree fairly well with each other.

When seepage occurs through the bottom boundary in an open channel, it has an influence on the water surface slope over the seepage region. The water surface slope can be evaluated using the water level elevations at the leading and the end section of the seepage region. For each section, a pitot-static

tube was used with a siphonic link to a container outside the flume. The water level elevations in the two containers were recorded at the same time to avoid possible error caused by water level fluctuations in the flume. A point gage with a vernier scale, which was used for the elevation measurement, was capable of reading the water level within an accuracy of ± 0.05 mm. The water surface slopes so obtained were assumed to represent those at the middle section of the seepage zone.

2.3 *Experimental procedure*

The sediment bed surface in the seepage region was first leveled to the elevation of the neighboring impermeable bed roughened by the same sediment. The pump for the seepage flow was then turned on and the seepage discharge was gradually adjusted to the predetermined value. Following this, the water for the main flow was slowly pumped to the head tank of the flume at a controlled rate. The tailgate was then adjusted to obtain the required water depth in the channel. To ensure a steady condition for each run, both the flowrates and the water depth were frequently checked and monitored during the test. Upon setting up the flowrates and water depth, velocity measurements were finally performed.

3 Experimental results and analysis

Table 1 summarizes the flow parameters for all the experiments. Altogether 106 test runs were conducted in this study. The seepage velocity, which was computed by dividing the seepage flow rate by the total cross sectional area of the recess, varies from 0 to 0.48 cm/s, of which the largest is less than 3% of the average channel velocity. Comparatively, the ratio of the seepage flow rate to the rate of the channel flow reaches up to 40%. In all the test, the bed sediment remained stationary as the threshold of sediment transport was not exceeded. The aspect ratio of flow ranges from 4.6 to 9.0. The Froude number, $Fr = U/(gh)^{1/2} = 0.19 \sim 0.45$ and the Reynolds number, $Re = \rho Uh/\mu = 2.7 \times 10^4 \sim 8.6 \times 10^4$, where h = water depth, U = depth-averaged velocity, g = gravitational acceleration, ρ = fluid density and μ = dynamic viscosity.

Table 1. Summary of experimental data.

Run No	x (cm)	h (cm)	U (cm/s)	v_s (cm/s)	B/h	$U/(gh)^{0.5}$	$\rho Uh/\mu$. (10^4)	Instrument
1~59	-20~170	7.8~15.4	20.4~45.2	0~0.476	4.6~9.0	0.19~0.45	2.7~7.2	Propeller
60~106	-30~230	13.1~15.1	26.6~52.1	0~0.475	4.6~5.3	0.22~0.44	4.7~8.6	ADV
Notes: d = 0.195 cm in Runs. 1 ~ 56 and 0.583 cm in Runs 57 ~ 106.								

3.1 *Mean velocity distribution*

The experimental data collected for flows with no seepage show that fully developed, rough turbulent flows were established over the sediment bed in the seepage zone. The profiles obtained follow approximately the logarithmic law of the wall:

$$\frac{u}{u_*} = 2.5 \ln \frac{y}{k_s} + 8.5 \tag{1}$$

where $u_* = \sqrt{\tau_b/\rho}$ = shear velocity; τ_b = bed shear stress; and k_s = equivalent sand roughness = $2d_{50}$.

In the presence of an upward seepage, flow over the permeable bed experiences an increased flow rate, which causes changes in the velocity distributions. Typical streamwise velocity distributions obtained from the study are plotted in Fig. 2, where x = distance measured from the leading edge of the seepage zone; U_o = depth-averaged velocity at the leading section of the seepage zone; and the subscript o denotes the section at $x = 0$. Only one series of data ($v_s/U_o = 0.0107$) are presented in this paper since the other results show similar behaviour. The curve superimposed in Fig. 2 represents the velocity distribution at $x = -10$ cm, which is obtained by fitting the measured data to the logarithmic law.

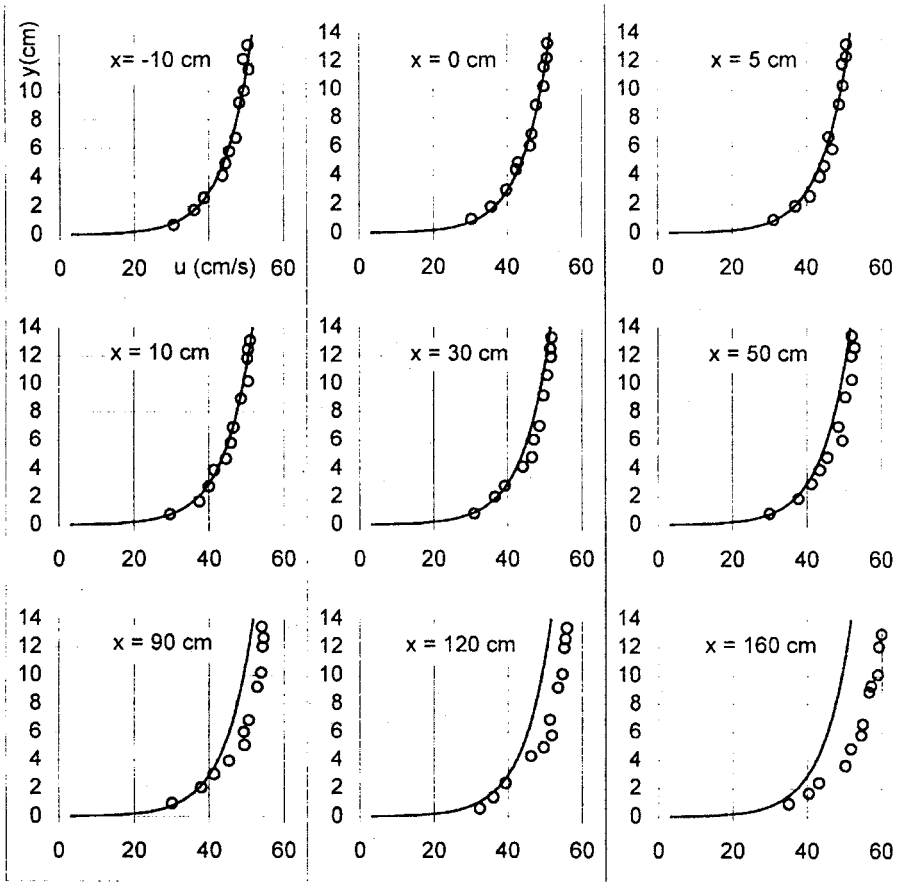

Fig. 2. Velocity profiles subjected to upward seepage ($v_s/U_o = 0.0107$).

Fig. 2 shows that the streamwise velocity increases in the downstream direction within the seepage zone. The increase is expected and it reflects the contribution of inflow from seepage. The measured velocity profiles also show that the increase is much more apparent in the upper portion of the profiles than that in the lower portion. To further illustrate this phenomenon, the values of velocities at three different depths, i.e., $y = 0.1h$, $0.5h$ and $0.9h$, are extracted from the measured velocity profiles in Fig. 2, and the data are then plotted against the streamwise coordinate in Fig. 3.

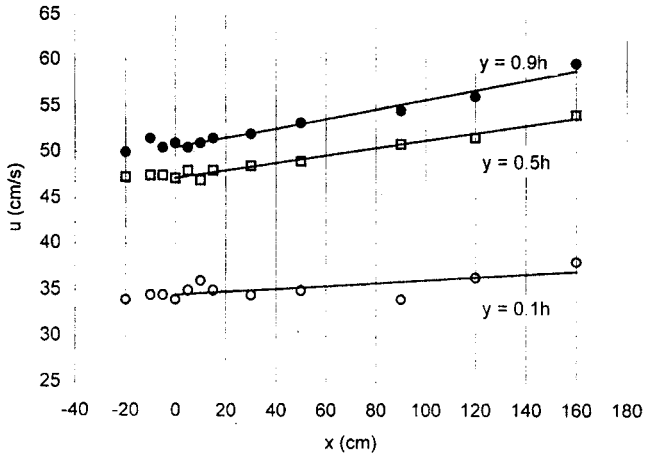

Fig. 3. Velocity increases at different depths.

Fig. 3 shows an obvious increase of the streamwise velocity at $y = 0.9h$; but comparatively less apparent in the near-bed layer. This change implies that the upward seepage causes the near-bed layer to deviate from its original path towards the surface layer, resulting in the development of an internal boundary layer. The average velocity variations in the downstream direction at the specified depths can be computed from Fig. 3 by assuming the variations to be linear. The data tabulated in Table 2 show that the velocity variations (du/dx) in the surface layer ($y = 0.9h$) is 0.051 sec^{-1}, and it reduces to 0.015 sec^{-1} in the near-bed layer ($y = 0.1h$). Table 2 also includes the variations of the dimensionless velocity for comparison. They are computed from a dimensionless plot of u/U against x/L as shown in Fig. 4, where U = local depth-averaged velocity and L = length of the seepage zone. Fig. 4 shows that the dimensionless streamwise velocity at $y = 0.9h$ increases slightly, but that near the bed layer ($y = 0.1h$) decreases in the downstream direction.

Table 2. Seepage effect on flow characteristics at specified depths.

y/h	du/dx (s^{-1})	$\frac{d(u/U)}{d(x/L)}$	du'_{rms}/dx (s^{-1})	$\frac{d(u'_{rms}/U)}{d(x/L)}$	dv'_{rms}/dx (s^{-1})	$\frac{d(v'_{rms}/U)}{d(x/L)}$	$d(\overline{-u'v'})/dx$ (cm/s^2)	$\frac{d(\overline{-u'v'}/U^2)}{d(x/L)}$
0.1	0.015	-0.045	0.012	0.028	0.004	0.010	0.0282	0.0014
0.5	0.040	0.019	0.006	0.009	0.001	-0.002	0.0155	0.0007
0.9	0.051	0.054	0.001	-0.008	0.000	-0.006	0.0029	0.0000

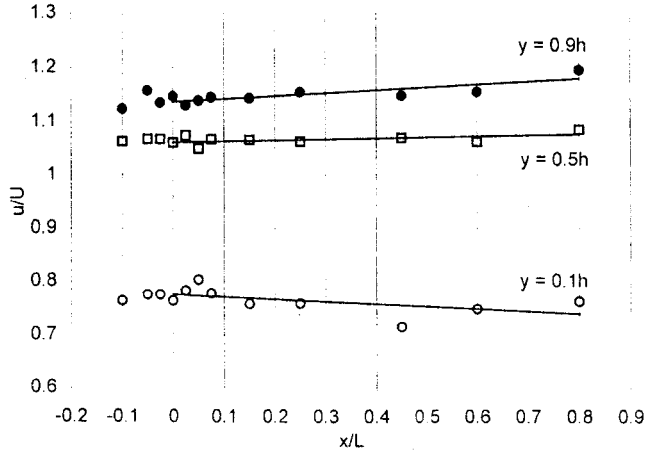

Fig. 4. Variations of dimensionless velocity at different depths.

3.2 *Turbulence intensities*

From the viewpoint of time-mean flow, the experimental data in Fig. 3 show that the presence of seepage results in an increase of flow rate in the streamwise direction. Besides this, seepage also causes a non-zero vertical velocity on the bottom boundary. With these changes, the properties of turbulence, i.e., turbulent intensity and Reynolds stress are expected to change. Typical profiles of the rms values of streamwise and vertical velocity fluctuations are shown in Figs. 5 and 6, where the same series of data used earlier is chosen.

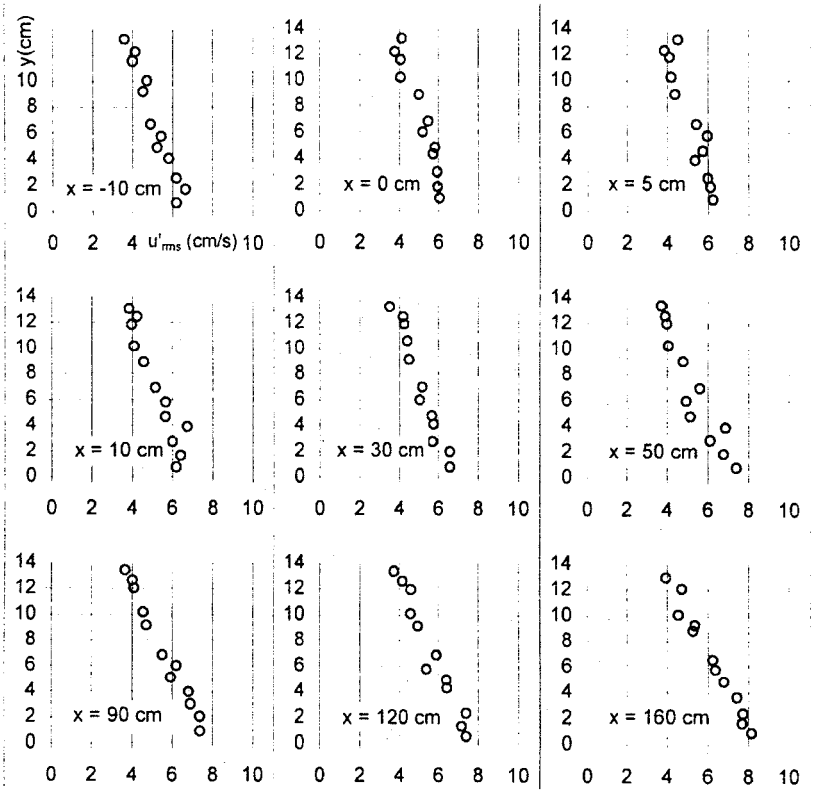

Fig. 5. Distributions of rms values of streamwise velocity fluctuations subjected to seepage ($v_s/U_o = 0.0107$).

With the upward seepage, the data show an increase of the rms values of velocity fluctuations near the bed in the downstream direction, but little change was observed for those in the surface layer. This phenomenon is in contrast to the changes of the time averaged streamwise velocity due to upward seepage. The latter increases much more in the surface layer. The data suggest that the seepage not only increases the flow rate in the channel, but also modifies the turbulent features even though the seepage velocity is very small compared with the channel velocity. As the upward seepage interferes with the channel flow immediately near the bed rather than the water surface, the turbulent features near the bed change more obviously.

Similar to the velocity changes drawn in Figs. 3 and 4, the rms values of the velocity fluctuations at $y = 0.1h$, $0.5h$ and $0.9h$ are also plotted in Figs. 7 and 8. The data plotted show different rates of increase of the rms values of the velocity fluctuations at different depths. The values evaluated from Figs. 7 and 8 are summarized in Table 2, which show significant levels of increase of u'_{rms} and v'_{rms} at $y = 0.1h$, whereas the rates of increase at $y = 0.9h$ are almost zero. Dimensionless distributions of the *rms* values of the velocity fluctuations at the specified depths are shown in Figs. 9 and 10, where u'_{rms}/U and v'_{rms}/U are plotted against x/L. The corresponding rates of increase are also

included in Table 2 for comparison. Contrary to the variations of the relative velocity u/U, the dimensionless variables u'_{rms}/U and v'_{rms}/U increase at $y = 0.1h$ but decrease at $y = 0.9h$.

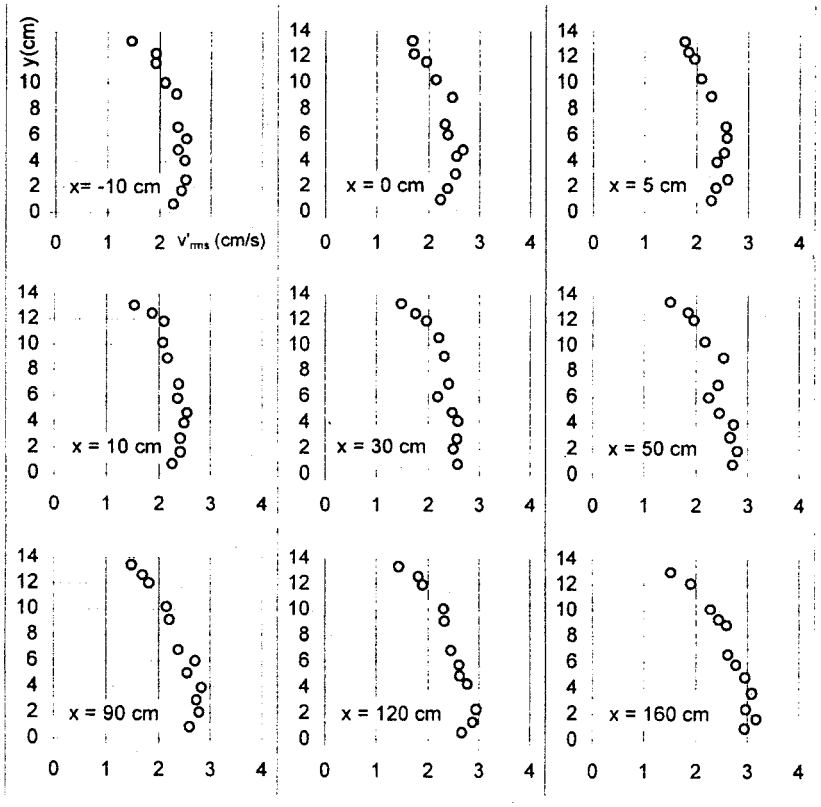

Fig. 6. Distributions of rms values of vertical velocity fluctuations subjected to seepage ($v_s/U_o = 0.0107$).

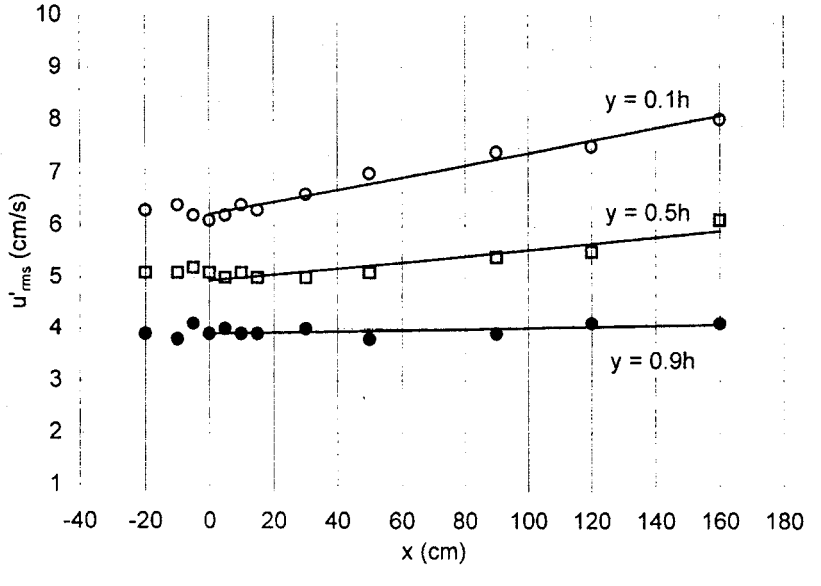

Fig. 7. Variations of streamwise velocity fluctuations at different depths ($v_s/U_o = 0.0107$).

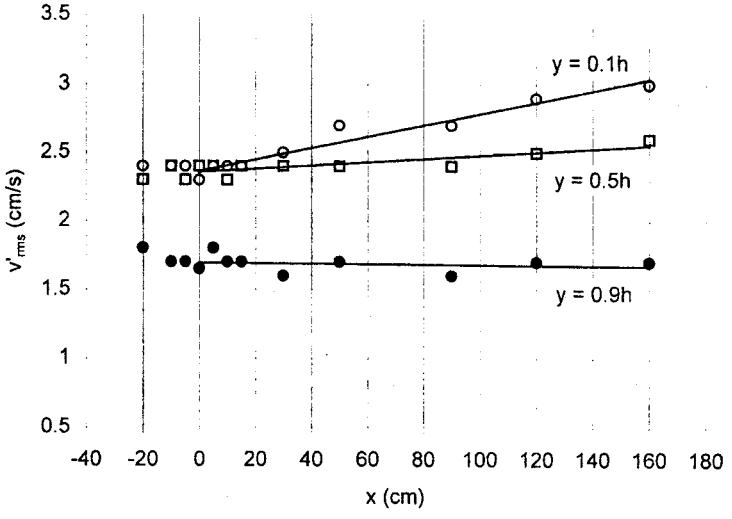

Fig. 8. Variations of vertical velocity fluctuations at different depths ($v_s/U_o = 0.0107$).

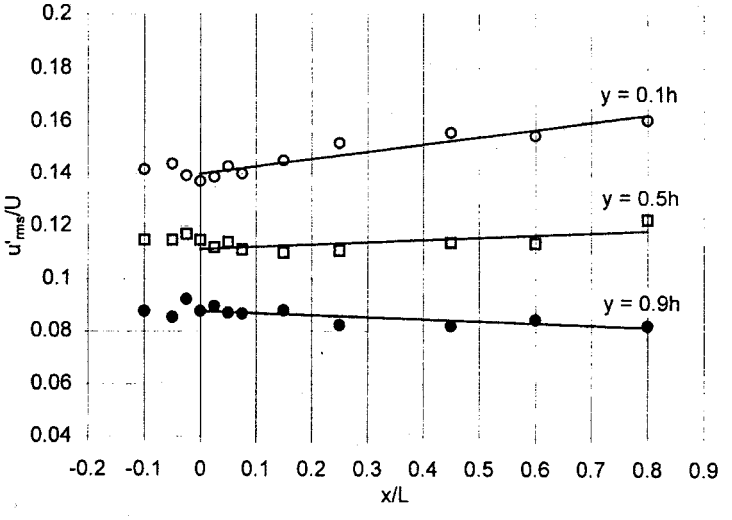

Fig. 9. Dimensionless streamwise velocity fluctuations at different depths ($v_s/U_o = 0.0107$).

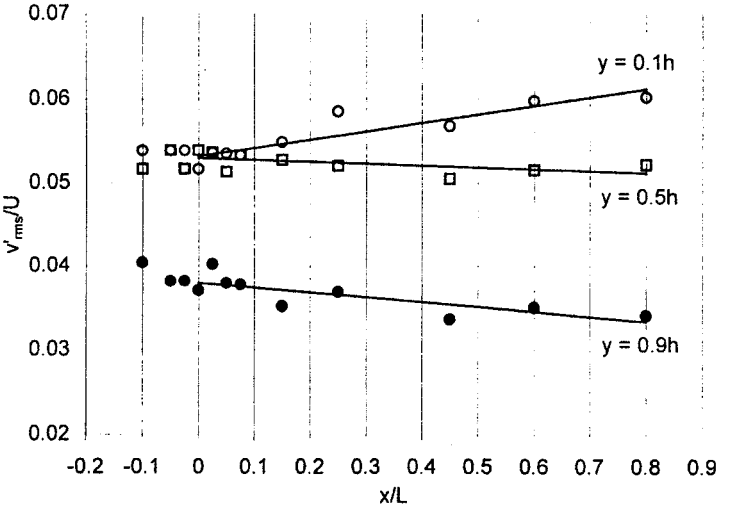

Fig. 10. Dimensionless vertical velocity fluctuations at different depths ($v_s/U_o = 0.0107$).

3.3 *Reynolds shear stress*

Fig. 11 shows the profiles of the Reynolds shear stress over the seepage zone. They exhibit similar variations as those in Figs. 5 and 6. However, the seepage effect on the Reynolds shear stress is more prominent, especially in the region near the bed. By extracting the values of the Reynolds shear stress at $y = 0.1h$, $0.5h$ and $0.9h$ from Fig. 11, its variations at those relative depths in the downstream direction are plotted in Fig. 12. The average rates of increase of the Reynolds shear stress is 0.028 cm/s^2 at $y = 0.1h$, and it becomes 0.003 cm/s^2 at $y = 0.9h$.

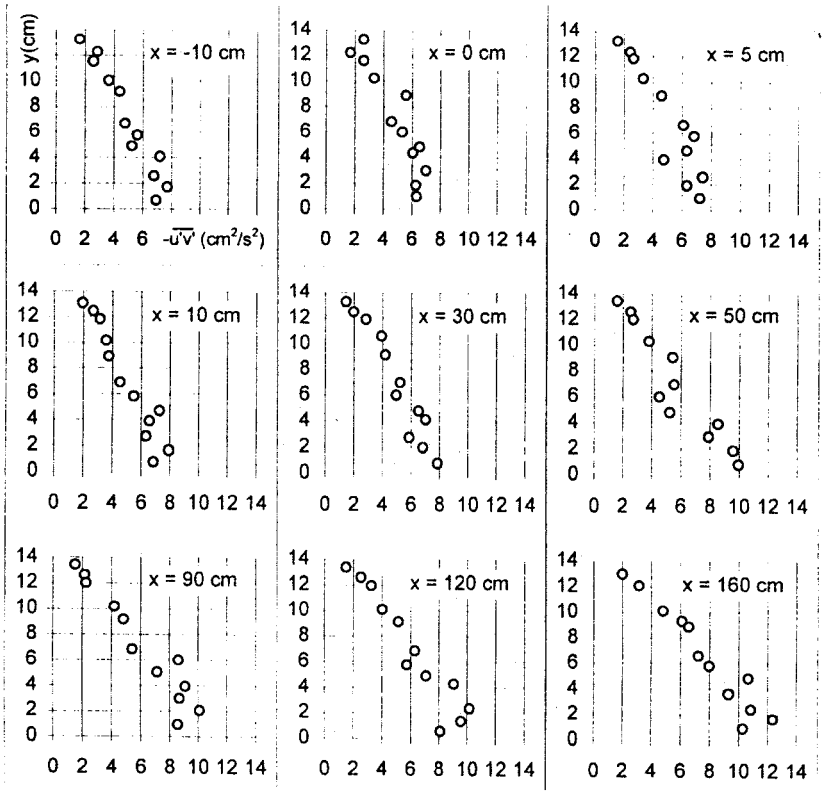

Fig. 11. Reynolds shear stress distributions subjected to upward seepage ($v_s/U_o = 0.0107$).

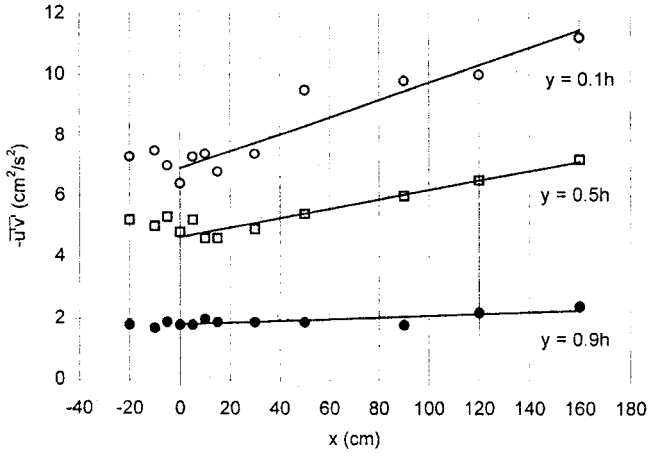

Fig. 12. Variations of Reynolds shear stress at specified depths ($v_s/U_o = 0.0107$).

Fig. 13 shows the relation of the dimensionless Reynolds shear stress $-\overline{u'v'}/U^2$ with x/L at the three specified depths. The related values of the increasing rates of the Reynolds shear stress, computed from Figs. 12 and 13, are tabulated in Table 2 and they show similar changes to those in the rms values of velocity fluctuations.

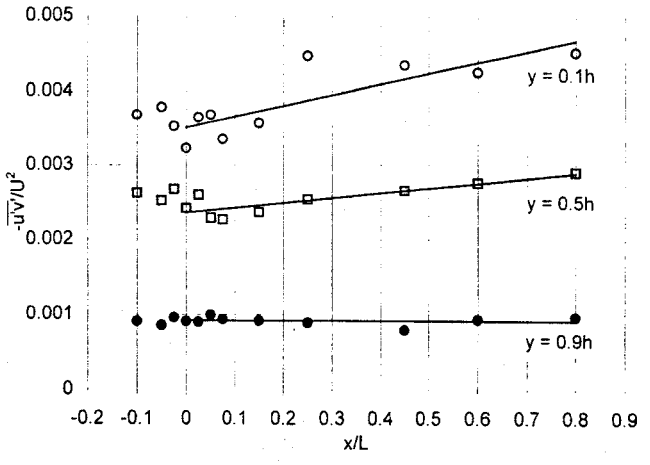

Fig. 13. Dimensionless Reynolds shear stress at different depths ($v_s/U_o = 0.0107$).

3.4 *Bed shear stress*

As the upward seepage causes significant changes in the near-bed turbulent velocity and the near-bed Reynolds shear stress, it should also affect the bed shear stress. For a two-dimensional open-channel flow without seepage, there are numerous methods available for the evaluation of the bed shear stress. One typical method is to compute the bed shear stress by fitting the logarithmic law of the wall to the measured velocity profiles. Another way is to measure the water surface slope S_w and to compute the bed shear stress according to $\tau_b = \rho g h S_w$. Still another is to directly measure the boundary shear stress using the Preston tube. When the profile of the Reynolds shear stress is available, the bed shear stress can also be estimated by extrapolating it to the boundary. In the presence of boundary seepage, the boundary conditions of the flow are changed. This change leads to the invalidation of all the above-mentioned methods except for the last one in evaluating the bed shear stress.

In this study, two approaches are adopted to compute the bed shear stress in the case of seepage. First, a momentum integral equation is derived from the controlling equations for the problem considered, so that the bed shear stress can be computed using the water surface slope, seepage velocity and other flow parameters. The bed shear stresses computed using the momentum integral equation are then compared with those obtained by the second method, i.e., by extending the Reynolds shear stress distributions to the boundary.

Momentum integral equations in the case of seepage. For a steady two dimensional, gradually varied open-channel flow, the controlling equations can be reduced to the form:

$$\frac{\partial u}{\partial x} + \frac{\partial u}{\partial y} = 0 \tag{2}$$

$$u\frac{\partial u}{\partial x} + v\frac{\partial u}{\partial y} = g\sin\phi_b - \frac{1}{\rho}\frac{\partial p}{\partial x} + \frac{1}{\rho}\frac{\partial \tau}{\partial y} \tag{3}$$

$$0 = -g\cos\phi_b - \frac{1}{\rho}\frac{\partial p}{\partial y} \tag{4}$$

where x, y denote the coordinates tangential and normal to the bottom boundary, respectively; u, v = the corresponding velocities in the x and y axes, respectively; ϕ_b = the angle of the bed plane to the horizontal; τ = total shear stress consisting of viscous shear stress and Reynolds shear stress; p = pressure; and g = gravitational acceleration. Fig. 14 shows the definition sketch for an open channel flow with seepage.

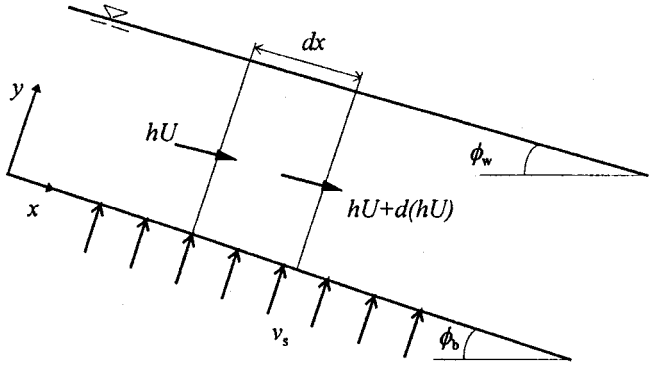

Fig. 14. Definition sketch for open channel flow with seepage.

Eqs. (2) through (4) can be integrated with the appropriate boundary conditions as follows:

$$u|_{y=0} = 0 \tag{5}$$

$$v|_{y=0} = v_s \tag{6}$$

$$p|_{y=h} = 0 \tag{7}$$

$$\tau|_{y=h} = 0 \tag{8}$$

$$u|_{y=h}\frac{dh}{dx} = v|_{y=h} \tag{9}$$

First, integration of Eq. (2) with respect to y yields the dept-averaged continuity equation:

$$\frac{d(hU)}{dx} = v_s \tag{10}$$

Eq. (4) integrates to the form:

$$p = \rho g(h-y)\cos\phi_b \tag{11}$$

By differentiating Eq. (11) with respect to x, one gets

$$\frac{\partial p}{\partial x} = \rho g \frac{dh}{dx} \cos\phi_b \tag{12}$$

Substituting Eq. (12) into Eq. (3) gives

$$u\frac{\partial u}{\partial x} + v\frac{\partial u}{\partial y} = g\sin\phi_b - g\frac{dh}{dx}\cos\phi_b + \frac{1}{\rho}\frac{\partial \tau}{\partial y} \tag{13}$$

Applying the continuity Equation (2), Eq. (13) can be rewritten as

$$\frac{\partial u^2}{\partial x} + \frac{\partial uv}{\partial y} = g\sin\phi_b - g\frac{dh}{dx}\cos\phi_b + \frac{1}{\rho}\frac{\partial \tau}{\partial y} \tag{14}$$

By integrating Eq. (14) with respect to y, one gets

$$\rho\int_o^h \frac{\partial u^2}{\partial x} dy + \rho(uv)|_{y=h} = \rho g h \sin\phi_b - \rho g h \frac{dh}{dx}\cos\phi_b - \tau_b \tag{15}$$

With the definition of the momentum correction factor

$$\beta = \left(\int_o^h u^2 dy\right) / (hU^2) \tag{16}$$

the terms on the left hand side of Eq. (15) can be transformed, with Eq. (9), to the form

$$\rho\int_o^h \frac{\partial u^2}{\partial x} dy + \rho(uv)|_{y=h} = \int_o^h u^2 dy = \rho\frac{d}{dx}(\beta h U^2) \tag{17}$$

Further, applying Eq. (10) to (17) leads to

$$\rho\int_o^h \frac{\partial u^2}{\partial x} dy = 2\beta\rho U v_s - \beta\rho U^2 \frac{dh}{dx} \tag{18}$$

Substituting Eq. (18) into (15), the bed shear stress subjected to seepage is expressed as

$$\tau_b = \rho u^2 = \rho g h \sin\phi_b - \rho g h \frac{dh}{dx}\left(\cos\phi_b - \frac{\beta U^2}{gh}\right) - 2\beta\rho U v_s \tag{19}$$

Eq. (19) shows that the bed shear stress is dependent on the depth-averaged velocity, water depth, water surface slope and seepage velocity. As is to be expected from its derivation, Eq. (19) reduces to the common momentum integral equation when the seepage velocity vanishes. For the case of a horizontal bed, $\phi_b = 0$, Eq. (19) reduces to

$$\tau_b = -\rho g h \frac{dh}{dx}\left(1 - \frac{\beta U^2}{gh}\right) - 2\beta\rho U v_s \tag{20}$$

Eq. (20) will be used to evaluate the bed shear stress in open-channel flow with a horizontal bed in the case of seepage.

Evaluation of bed shear stress. The precision of using Eq. (20) to compute τ_b is closely associated with the measurements of the water surface slope. As was described earlier, the water surface slopes were computed using the measured water level differences between the upstream and downstream ends of the seepage zone. As the water surface slopes over the seepage zone are not constant, these slopes so computed only approximate those at the middle section in the seepage zone. This limitation means that, with the computed slope, only the bed shear stress at the middle section over the seepage zone can be evaluated using Eq. (20).

To ensure that the computed bed shear stresses using the momentum integral equation are acceptable, it is necessary to compare them with those obtained using another independent approach. To do so, the measured Reynolds shear stress distribution at the middle section in the seepage zone is linearly extrapolated to the boundary, leading to the value of the bed shear stress for comparison. This is because when ignoring the viscous shear stress, the Reynolds shear stress is equal to the total shear stress, and it approaches the boundary shear stress, τ_b, especially for a small distance from the bed. The values of the bed shear stress derived based on the above two methods are tabulated in Table 3. They show a good agreement with an average discrepancy of 12%.

Table 3. Comparison of computed bed shear stress.

No	U (cm/s)	h (cm)	v_s (cm/s)	τ_{b1} (N/m^2)	τ_{b2} (N/m^2)	Error (%)
1	44.75	14.2	0.154	1.429	1.197	16.2
2	45.20	14.2	0.298	1.418	1.050	26.0
3	46.06	14.2	0.467	1.418	1.096	22.7
4	28.93	14.9	0.438	0.462	0.458	0.9
5	27.45	14.9	0.223	0.544	0.520	4.5
6	31.55	13.1	0.223	0.571	0.645	-12.9
7	37.06	13.1	0.448	0.704	0.650	7.6
8	47.26	14.7	0.471	1.374	1.444	-5.1
9	47.56	14.4	0.475	1.148	1.190	-3.7
10	46.57	14.4	0.219	1.476	1.218	17.5

Notes: The values of τ_{b1} were computed using Eq. (20) and those of τ_{b2} were obtained by extrapolating the measured Reynolds shear stress distributions to the boundary.

Reduction of bed shear stress. Fig. 15 shows the effect of upward seepage, where the relative bed shear stress τ_b/τ_{bo} is plotted against the relative seepage velocity v_s/U. Here, the bed shear stress with seepage τ_b is evaluated by using Eq. (20) and τ_{bo} denotes the bed shear stress with no seepage for the same water depth, depth-averaged velocity and bed sediment.

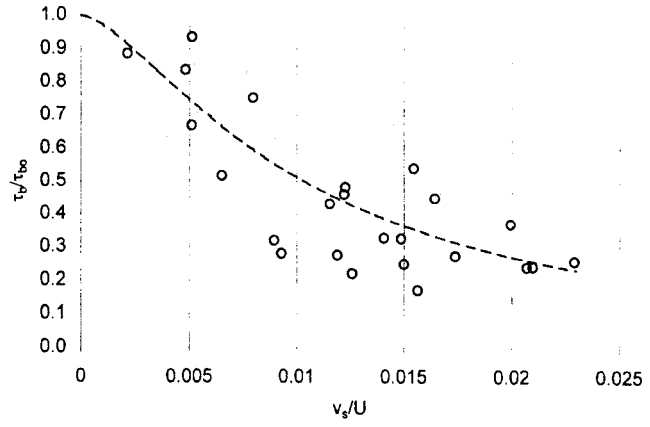

Fig. 15. Decreased bed shear stress due to upward seepage.

The latter was computed using the following equation:

$$\tau_b = \rho u_{*_o}^2 = \frac{\rho U^2}{6.25 \ln^2(11h/k_s)} \tag{21}$$

Eq. (21) can be derived by integrating Eq. (1) from $y = 0$ to $y = h$. For zero seepage, the bed shear stresses computed using Eq. (21) are close to those computed using Eq. (20).

The experimental data show that with increasing relative seepage velocity, v_s/U, the relative bed shear stress decreases. The bed shear stress is reduced by approximately 50% for the seepage ratio of 1%, and by approximately 75% for the seepage ratio of 2%.

A consistent conclusion with the results in Fig. 15 has been drawn from previous investigations in aerodynamics, such as Clarke et al. (1955) and Turcotte (1960). Their studies have shown that the skin friction in the boundary layer, when an injection is applied through the porous boundary, reduces in comparison with those without injection. Fig. 16 provides a comparison of the present experimental results with Turcotte's study that was conducted in the case of a smooth permeable boundary. Turcotte's results show a faster decrease of the boundary shear stress due to injection, as compared to the experimental results obtained for a rough boundary in the present study. The latter shows that with a rough sediment bed, the seepage-induced reduction of the bed shear stress becomes much gentler.

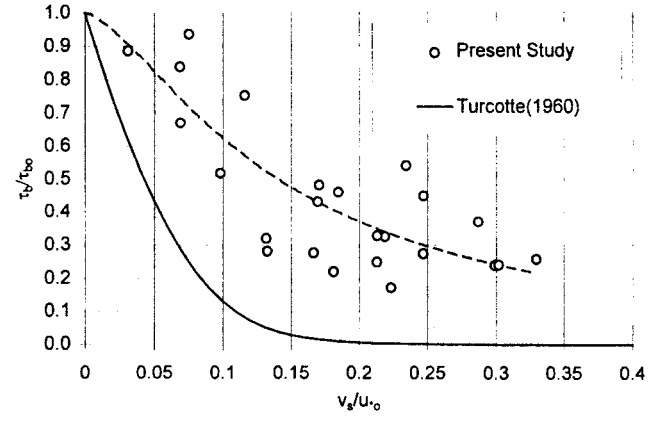

Fig. 16. Comparison of the present study and Turcotte (1960)'s study.

4 Conclusions

This study presented the experimental measurements conducted in open channel flow with an upward seepage. The results show that the upward seepage affects the velocity profiles, the rms values of velocity fluctuations, the Reynolds shear stress and the bed shear stress.

With an upward seepage, the increase of the time-mean streamwise velocity is more apparent near the free-surface than that near the permeable bed. On the other hand, the rms values of the velocity fluctuations and the Reynolds shear stress exhibit opposite variations, they increase more rapidly near the bed than that near the surface layer of the flow. The levels of the various increases are reduced if the flow parameters considered are normalized based on the depth-averaged velocity at the local sections over the seepage zone.

Upward seepage also leads to a reduction of the bed shear stress. The experimental data show that the reduction becomes much gentler for a rough sediment bed, as compared with the previous study for a smooth permeable boundary. The bed shear stresses computed using the momentum integral equation are in a good agreement with those obtained by extrapolating the measured Reynolds shear stress profiles to the boundary.

Acknowledgements

The writers appreciate the helpful comments from Prof. Gary Parker, St. Anthony Falls Hyd. Lab., Dept. of Civil and Min. Eng., Univ. of Minnesota, USA.

Notations

d_{50} median diameter of sediment particles
g gravitational acceleration
h water depth
h_o water depth at the starting section of seepage zone
k_s equivalent sand roughness
L length of the seepage zone
p pressure
u time-mean streamwise velocity
u_* $\sqrt{\tau_b/\rho}$ = shear velocity
u_{*o} $\sqrt{\tau_{bo}/\rho}$ = shear velocity without seepage
u'_{rms} *rms* value of streamwise velocity fluctuations
U depth-averaged velocity
U_o depth-averaged velocity at the leading section of the seepage zone
v time-mean normal velocity
v'_{rms} rms value of normal velocity fluctuations
v_s seepage velocity
x streamwise coordinate or streamwise distance from the leading edge of seepage zone
y normal coordinate or normal distance from the bed surface
β momentum correction factor
ρ density of fluid
$-\rho\overline{u'v'}$ Reynolds shear stress
τ shear stress

τ_b bed shear stress
τ_{bo} bed shear stress without seepage
ϕ_b angle of bed slope

References

CLARKE, J. H., MENKES, H. R., and LIBBY, P. A. (1955). "A provisional analysis of turbulent boundary layers with injection." J. Aerospace Sciences, 22(4), 255–260.

KRAUS, N. C., LOHRMANN, A., and CABRERA, R. (1994). "New acoustic meter for measuring 3D laboratory flows." J. Hydr. Eng., ASCE, 120(3), 406–412.

MACLEAN, A. G. (1991a). "Open channel velocity profiles over a zone of rapid infiltration." J. Hydr. Res., 29(1), 15–27.

MACLEAN, A. G. (1991b). "Bed shear stress and scour over bed-type river intake." J. Hydr. Eng., ASCE. 117(4), 436–451.

OLDENZIEL, D. M., and BRINK, W. E. (1974). "Influence of suction and blowing on entrainment of sand particles." J. Hydr. Div., ASCE, 100(7), 935–949.

PRINOS, P. (1995). "Bed-suction effects on structure of turbulent open-channel flow." J. Hydr. Eng., ASCE, 121(5), 404–412.

TURCOTTE, D. L. (1960). "A sublayer theory for fluid injection into incompressible turbulent boundary layer." J. Aerospace Sciences, 27(9), 675–678.

WILLETTS, B. B., and DROSSOS, M. E. (1975). "Local erosion caused by rapid forces infiltration." J. Hydr. Div., ASCE, 101(12), 1477–1488.